Desalination and Water Treatment
www.deswater.com
doi: 10.1080/19443994.2014.916233

55 (2015) 539–548
June

Taylor & Francis
Taylor & Francis Group

Removal of methylene blue from aqueous solution using humic-acid coated magnetic nanoparticles

Rong Ping Chen[a], Yin Long Zhang[b,*], Xiao Yan Wang[c], Cheng Yue Zhu[a], Ai Jun Ma[d], Wei Min Jiang[d]

[a]*School of Chemical Engineering, Nanjing Forestry University, Nanjing 210037, P.R. China, emails: chenrongping2000@163.com (R.P. Chen), zhuzhuaggie@126.com (C.Y. Zhu)*
[b]*School of Forest Resource and Environment, Nanjing Forestry University, Nanjing 210037, P.R. China, Fax: +86 25 85427045; email: ylzhang@njfu.edu.com*
[c]*Department of Science and Technology, Nanjing Forestry University, Nanjing 210037, P.R. China, email: ecoenvylz@163.com*
[d]*Jiangsu Polytechnic College of Agriculture and Forestry, Jurong 212400, P.R. China, emails: maaijun2@163.com (A.J. Ma), weimin6234@sina.com (W.M. Jiang)*

Received 10 February 2014; Accepted 12 April 2014

ABSTRACT

In this paper, magnetic Fe_3O_4/HA nanoparticles (MHA) were synthesized using a coprecipitation method. The structure and properties of the MHA were characterized by Fourier transform infrared spectroscopy, TG, transmission electron microscope, zeta potential, X-ray diffraction, and vibration sample magnetometer. MHA is proven to be stable in water and can be easily separated from solution under an external magnetic field. Adsorptive removal of methylene blue (MB) from aqueous solution using MHA was systematically studied. The fundamental adsorption experiments reveals that MHA is more efficient in dye removal when initial solution pH is higher than 4.0. The theoretical maximal adsorption capacity, which is based on the simulation results from the isothermal equilibrium study, is 200 mg/g. The adsorption kinetic and equilibrium behaviors of MHA are in agreement with pseudo-second-order model and Langmuir model, respectively. The value of activation energy (E_a) indicates that the adsorption of MB onto MHA is a physical process. The Gibbs free energy of the adsorption process (ΔG) is negative, indicating that the adsorption of MB onto MHA is thermodynamically favorable. Furthermore, MHA could be easily regenerated and reused with almost no loss of adsorption capacity, which is satisfactory for practical applications.

Keywords: Humic acid; Fe_3O_4 magnetic nanoparticles; Methylene blue; Adsorption

1. Introduction

Dye is a class of pollutant that is found in the effluents of textile, paper, plastic, food, and cosmetic industries [1]. The high chromaticity impedes light penetration and thus prohibits aquatic photosynthesis. Some of them are also able to chelate metal ions, resulting in micro-toxicity to fish and other water organisms [2]. Besides, many dyes are toxic or carcinogenic [3,4]. Considering the hazard of dyes, study on

*Corresponding author.

the removal of dyes from water body is of great environmental significance at present.

Nowadays, various techniques are employed in dye effluent treatment, such as adsorption, flocculation, chemical oxidation, electrochemical oxidation, and photocatalytic oxidation [5–12]. Among these techniques, adsorption shows multiple advantages due to its high efficiency in treating low concentration sewages, simple process, and reusability [13]. Yet conventional adsorbents still bear some disadvantages such as risk of secondary pollution and poor biodegradability [1].

In recent years, natural polymeric materials, such as humic acid (HA), starch, cellulose, and chitin, stand out as candidates for conventional adsorbents since they are easily accessible, inexpensive, biodegradable, nontoxic, and modifiable [14]. HA is a class of natural organic polymers which originates from the decomposition of plants and animal residues. HA exhibits fine reaction activity for bearing abundant functional groups such as carboxyl, phenolic, carbonyl, and amino groups [14], most of them are anionic. These groups make it easy for HA to bind cationic species from aqueous solutions.

In recent years, magnetic separation techniques is enjoying widening application in water treatment due to its great significance in enhancing separation efficiency and treating efficiency of small-sized adsorbents [15]. These adsorbents are in sizes of micrometer or nanometer scale. Despite their high adsorption efficiency, their separation becomes cumbersome when using traditional methods such as simple sedimentation and filtration. With magnetism impregnated, adsorbents could be readily separated from the water under external magnetic fields. Usually the impregnation is achieved by compositing magnetic substances into adsorbents. In this work, magnetism is also introduced to the nanoparticles.

In this study, a low-cost and environment-friendly magnetic adsorbent, magnetic Fe_3O_4/HA nanoparticles (MHA), was prepared by coprecipitation method, and applied to the removal of a common dye, methylene blue (MB) from water body. Physiochemical characterizations of synthesized MHA were performed using various modern analytical methods. Adsorption behaviors of MHA, including the effect of the initial solution pH, adsorption kinetics, and isothermal adsorption equilibrium, were investigated. In addition, recycling and reuse of the disused adsorbents were also carried out for evaluating its application potential.

2. Experimental

2.1. Materials

HA was purchased from Aladdin Industrial Corporation. Iron(III) chloride hexahydrate and Iron(II) sulfate heptahydrate were purchased from Sinopharm Chemical Reagent Co. Ltd, China. Ammonia solution (25%), Hydrochloric acid (HCl), sodium hydroxide (NaOH), and acetic acid were supplied by Shanghai Chemical Reagent Co. Ltd, China. MB was supplied by Tianjin Institute of Chemical Reagents. All the reagents used in this work are AR grade. Deionized water was used in all experiments.

2.2. Preparation of the adsorbent

HA coated Fe_3O_4 magnetic nanoparticles were prepared according to the methods by Liu et al. [16]. About 6.1 g of $FeCl_3{\cdot}6H_2O$ and 4.2 g of $FeSO_4{\cdot}7H_2O$ were dissolved in 100 mL of water and the resultant solution was heated to 90˚C, then 10 mL of ammonium hydroxide (25%) was added rapidly, followed by the addition of 50 mL of HA (1%, neutralized by NaOH). The mixture was then stirred at 90˚C for 30 min and cooled to room temperature afterwards. The resultant black precipitates were collected under a magnetic field and washed to neutral with distilled water. The resultant black precipitate is magnetic Fe_3O_4/HA nanoparticles (MHA) and it was stored for further use. Control samples, namely pristine Fe_3O_4 nanoparticles were prepared in a similar way without adding HA.

2.3. Characterization of the adsorbent

2.3.1. Fourier transform infrared spectroscopy

The Fourier transform infrared spectroscopy (FTIR) spectra of MHA, pristine Fe_3O_4, and pure HA were recorded using a Fourier transform infrared spectrometer (Avatar 360; Nicolet Co.; USA). All samples were pretreated as KBr tablets, and the range of scanning wave number is 500–4,000/cm.

2.3.2. Zeta potential analysis

The zeta potential of MHA at various solution pH was measured on a Zetasizer Analyzer (Nano ZS90; Malvern Co.; UK). The range of solution pH was about 2–9.

2.3.3. Vibration sample magnetometer

A vibrating sample magnetometer (MPMS-XL7; Quantum Design; USA) was used to characterize the

magnetic properties of MHA and pristine Fe_3O_4 at room temperature.

2.3.4. Transmission electron microscope

The transmission electron microscope (TEM) image of MHA was taken on a TEM (JEM-2100; JEOL Co. Ltd; Japan). The acceleration voltage was 25.0 kV. The sample was embedded in epoxy resin and then cut into ultrathin slices for analysis as it is magnetic. Magnetic materials were easily affected by electromagnetic field in the microscope, resulting in undesired movement of material, leading to analytical difficulty and risk of device breaking down.

2.3.5. Thermogravity analysis

Thermal stability of MHA, pristine Fe_3O_4, and pure HA were analyzed by a thermogravimetric analyzer (STA-449C; Netzsch Instrument Co. Ltd; Germany) in nitrogen atmosphere (the flow rate is 50 cm^3/min). The temperature was ranged from 25 to 800℃ at a scanning rate of 10˚/min.

2.3.6. X-ray diffraction

X-ray diffraction (XRD) patterns of MHA and pristine Fe_3O_4 were obtained using a X-ray diffractometer (Ultima IV; Rigaku Co. Ltd; Japan) with Cu K radiation. The data were collected in the range of 2θ between 10˚ and 100˚ at a scanning speed of 5˚/min.

2.3.7. Cation exchange capacity measurement

The cation exchange capacity of MHA is determined using $BaCl_2$ method [17]. Two grams of MHA is firstly equilibrated in excessive 0.1 M $BaCl_2$, Ba-loaded MHA (Ba-MHA) is centrifuged and washed several times with a certain volume of 2 mM $BaCl_2$. Then Ba-MHA is suspended and equilibrated in a certain volume of 5 mM $MgSO_4$, the conductivity of the supernatant is measured and compared with a reference 1.5 mM $MgSO_4$ solution, then a proper amount of 0.1 M $MgSO_4$ solution is added to make the conductivity of the supernatant equal to the reference solution. The cation exchange capacity is calculated based on the precipitation reaction of $BaSO_4$.

2.4. Batch adsorption experiments

2.4.1. Effect of initial solution pH

The influence of different initial solution pH was investigated at 25℃. Initial solution pH of the dye solutions ranged from 2.0 to 10.0, adjusted using HCl or NaOH solutions. In this experiment, 0.08 g (dry weight) of MHA was immerged in 80 mL of MB solution and stirred for 24 h to reach the equilibrium. The initial concentration of MB was 400 mg/L, based on adsorption isotherms.

MB concentration was analyzed by a Victor 722 Vis Spectrometer at 662 nm. Proper dilution was performed to ensure that the dye concentration of the solution was within the range of the standard curve before measurement. Adsorption capacity in subsequent experiments, q_e (mg/g), was calculated according to the following equation unless noted.

$$q_e = \frac{(C_0 - C_e)V}{m} \tag{1}$$

where C_0 and C_e (mg/L) are the initial and equilibrium MB concentrations in solution, respectively; V (L) is the volume of solution; m (g) is the weight of dry adsorbents.

2.4.2. Adsorption kinetics

Kinetic adsorption experiments were performed at initial pH 7.0. The initial concentration of MB solution was the same as in section 2.4.1 0.5 g of adsorbent was immerged into 500 mL MB solution under continuous agitation. Then, 1 mL of sample solutions was taken out at certain time intervals to measure MB concentration. Meanwhile, equivalent volume of water with pH 7.0 was added into the bulk solutions to maintain the solution volume [1].

The dye uptake $q(t_i)$ (mg/g) at time t_i was calculated using the following equation:

$$q(t_i) = \frac{(C_0 - C_{t_i})V_0 - \sum_2^{i-1} C_{t_{i-1}} V_a}{m} \tag{2}$$

where C_0 and C_{t_i} (mg/L) are the initial dye concentration and the concentrations at the time t_i, respectively. V_0 and V_a (L) are the volume of the mixed solution and the volume of the sample solution taken out at t_i for analysis, respectively. In this case, V_a equals to 1.0 mL and m (g) represents the weight of the adsorbent.

2.4.3. Adsorption isotherms

Adsorption equilibrium study for removal of MB dye was conducted at initial solution pH 7.0 and the concentrations of MB solutions ranged from 20 to 400

mg/L. About 0.08 g of MHA adsorbent was immerged into 80 mL of MB dye solution under continuous stirring. The same method as mentioned in the previous section was employed to analyze the initial and final MB concentrations. Adsorption capacity of MB was calculated according to Eq. (1).

2.4.4. Regeneration experiments

Regeneration and reuse of adsorbents is of great importance in practical applications. In this experiment, 2 mol/L KCl solution was selected as the regeneration agent to recover the dye-loaded adsorbents. The dye-loaded adsorbents washed with excess 2 mol/L KCl solution until no dye color in the effluent is observed. The recovered adsorbent was then washed by water, reactivated by 0.1 mol/L NaOH aqueous solution and subsequently washed again by deionized water. Finally, the regenerated adsorbent underwent the next adsorption–regeneration cycle. The experiment was conducted for five cycles. The dye adsorption capacity of MHA in the first cycle is set as 100% and the recycle efficiency (%) of regenerated MHA equals the ratio of the dye adsorption capacity in the current cycle to the capacity in the first cycle.

3. Results and discussion

3.1. Characterizations of MHA

FTIR spectra of MHA, pristine Fe_3O_4, and pure HA are shown in Fig. 1. For pristine Fe_3O_4 and MHA, the peak at 582/cm corresponds to the characteristic stretching vibration of the Fe–O bond [18]. The band at 1,630/cm of MHA is ascribed to the C=O stretching band, indicating the carboxylate anion interaction with the ferroxide surface [18,19]. The band at 1,400/cm can be ascribed to CH_2 scissoring [20]. The band at 1,110/cm is the C–O stretching of COO^-. Previous studies indicate that the binding of HA to Fe_3O_4 surface is mainly achieved through coordination [16,20]. It can be conclude that the carboxylate groups interact with FeO surface and play an important role in the bonding of the HA with the magnetite surface.

Zeta potentials of the MHA were measured at various pH and shown in Fig. 2. In Fig. 2, it is observed that the isoelectric point of MHA is approximately at pH 3.2 due to the carboxyl groups on HA coating [21]. According to a report, the zeta potential of pure HA is negative in the pH range of 0.5–9.5 [21]. Zeta potential of pristine Fe_3O_4 is positive below pH~7 and negatively above the point [22]. The zeta potential plot of MHA suggests that HA is coated on Fe_3O_4 surfaces. It also indicated that MHA is negatively charged at the environment of pH 3.2–9.5, which impedes the aggregation of MHA nanoparticles and is also beneficial for the adsorption of cationic species. Illes and Tombacz indicated that the colloidal stability of Fe_3O_4 nanoparticles coated with HA in aqueous solution is enhanced [23].

As observed in Fig. 3, the saturation magnetization of MHA and pristine Fe_3O_4 is 62.88 and 69.58 μ/g, respectively. The relatively high magnetization value makes the separation of MHA from its aqueous dispersions under an external magnetic field easy. MHA can quickly aggregate in the magnetic field and then achieve separation.

Fig. 4 demonstrates the TEM image of MHA. It is observed that the Fe_3O_4 particles in MHA has a quasi-spherical structure feature with particle size of about

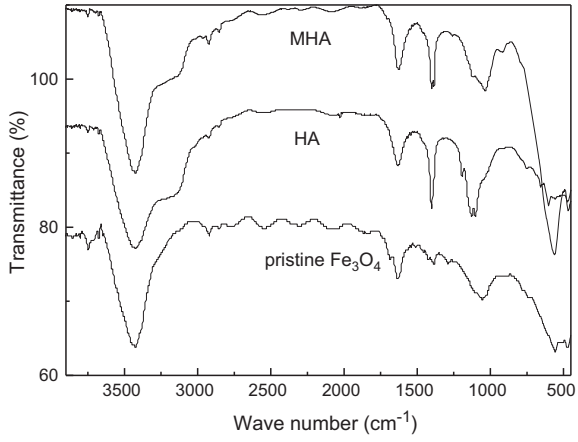

Fig. 1. FTIR spectra of MHA, pristine Fe_3O_4, and HA.

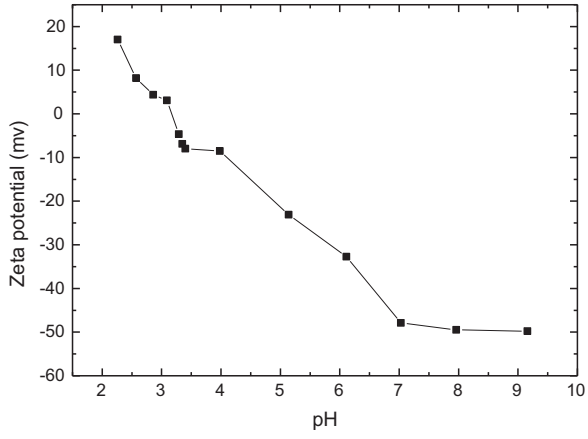

Fig. 2. Zeta potential curve of MHA at different initial solution pH.

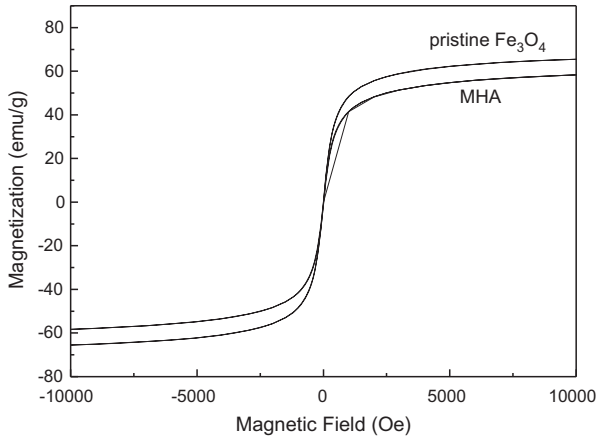

Fig. 3. Magnetization curves of MHA and pristine Fe_3O_4.

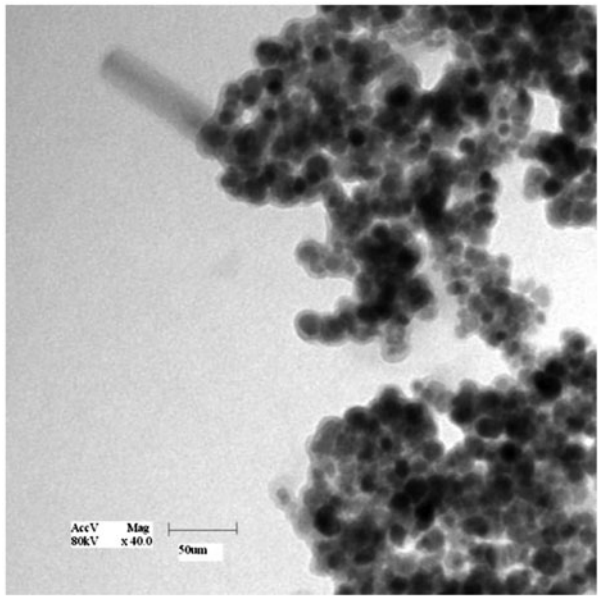

Fig. 4. TEM image of MHA nanoparticles.

10 nm, while the HA coating on MHA is amorphous on observation. Illes and Tombacz [24] reported that the primary size of Fe_3O_4 magnetite particles is less than 10 nm with an average aggregate size around 100 nm in the stable solutions. Niu et al. [25] also observed that MHA has nearly uniform distribution of particle size (10–12 nm) but Fe_3O_4 nanoparticles have no uniform size.

The TG curve of MHA is shown in Fig. 5. As observed, the weight loss at 350 °C is due to decomposition, dehydration, and carbonization of HA. As the weight loss of pristine Fe_3O_4 is rather small, it is neglected for calculation convenience. The content of

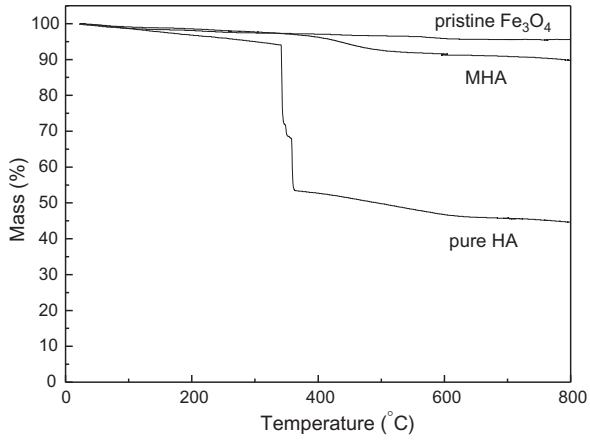

Fig. 5. TG curves of pristine Fe_3O_4, MHA, and HA.

HA in MHA is calculated based on the ratio of HA weight loss and MHA weight loss. According to these results, MHA contains about 18% HA and 82% Fe_3O_4, which is relatively close to the HA content in other materials that have been reported [18].

XRD patterns of pristine Fe_3O_4 and MHA were shown in Fig. 6. The two samples of pristine Fe_3O_4 and MHA have similar characteristic diffraction peaks at $2\theta = 30.3°$, 35.4°, 42.6°, 53.9°, 57.2°, 62.8°, which correspond to the characteristic (220), (311), (400), (422), (511), and (440) planes of cubic Fe_3O_4 phase with a spinel structure (JCPDS No. 85-1436) [22]. There is no distinct difference between the nanoparticles of Fe_3O_4 and MHA, indicating that the crystal structure of Fe_3O_4 in MHA is maintained after coating with HA.

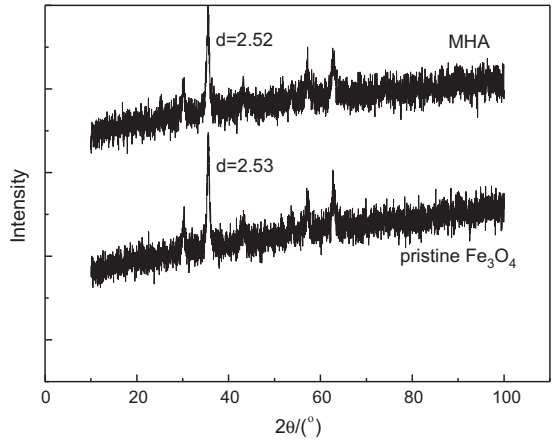

Fig. 6. XRD patterns of pristine Fe_3O_4 and MHA.

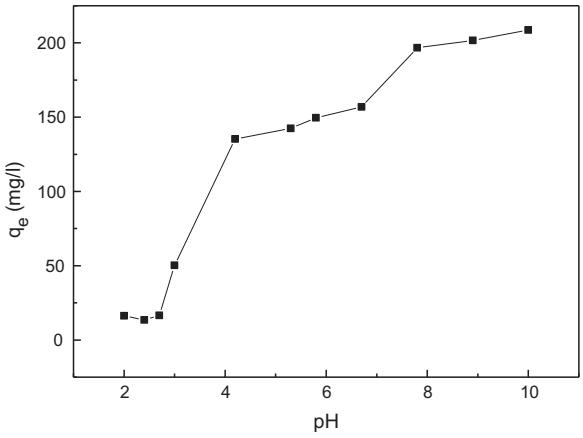

Fig. 7. Effect of initial solution pH on MB adsorption onto MHA.

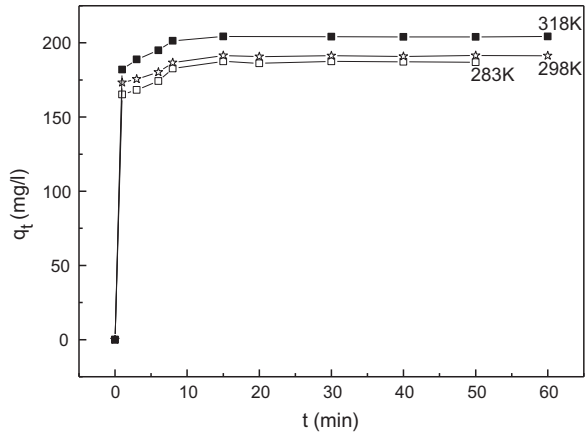

Fig. 8. Adsorption capacity time dependence of MB onto MHA (initial MB concentration 400 mg/L; solution pH 7.0).

3.2. Adsorption experiments

3.2.1. Effect of initial solution pH on MB adsorption

The plot of adsorption capacity vs. initial pH is shown in Fig. 7. The upper limit of studied pH is set at 10 since at pH higher than 10, the adsorption behavior becomes difficult to interpret, as many cationic dyes are unstable under strong alkaline conditions and dyes would precipitate [26]. As is shown in Fig. 7, the adsorption of MB on the surface of MHA is greatly influenced by initial solution pH. MHA exhibits efficient MB removal in the initial solution pH range of 4–10, where the adsorption capacity is about 140–200 mg/g. The adsorption to MB is weak in solutions whose initial pH is lower than 4, which is due to the protonation of the anionic groups on MHA. When the pH is higher than the isoelectric point of MHA, the surface of MHA becomes negatively charged, as the surface carboxyl groups deprotonate. The negatively charged MHA can better react with cationic MB through electrostatic attraction and MB removal thus becomes efficient. According to cation exchange capacity analysis, the capacity of MHA is about 80 mmol/100 g, about 75–80% of its exchanging sites is occupied by MB when the MB adsorption on it reaches saturation.

Safarik et al. [27] reported that the magnetic particles may partially dissolve with magnetism loss in strongly acidic solutions. Whereas no signification change of MHA in acidic environment was observed in this experiment, which is due to the protection from HA coating [28]. Besides, HA coating can also enhance the endurance of Fe_3O_4 nanoparticles towards oxidation.

3.2.2. Adsorption kinetics

The kinetic adsorption results were shown in Fig. 8. It is observed that the adsorption equilibrium of MHA for MB is achieved within about 15 min. The short equilibrium time indicates high adsorptive reaction rate of MHA, which is significant in practical applications.

To further study the adsorption mechanism, three kinetic models are used to simulate the kinetic data, namely pseudo-first-order, pseudo-second-order, and intraparticle diffusion models.

The pseudo-first-order kinetic model is expressed as the following equation [29]:

$$\ln(q_e - q_t) = \ln q_e - k_1 t \tag{3}$$

where k_1 (min^{-1}) is the rate constant of pseudo-first-order adsorption; q_e and q_t (mg/g) are the amount of MB absorbed onto adsorbents at equilibrium and at time t (min), respectively.

The pseudo-second-order kinetic model can be expressed Eq. (4) [30]:

$$\frac{t}{q_t} = \frac{1}{k_2 q_e^2} + \frac{t}{q_e} \tag{4}$$

where q_e and q_t (mg/g) are the amounts of MB adsorbed onto adsorbents at equilibrium and at time t (min), respectively; k_2 (g/(mg min)) is the rate constant of pseudo-second-order model.

Intraparticle diffusion model suggests that intraparticle diffusion is the rate-limiting step in the

Table 1
Kinetic parameters for MB onto MHA

	Pseudo-first-order model				Pseudo-second-order model			Intraparticle diffusion model		
T(K)	$q_{e,\mathrm{exp}}$ (mg/g)	k_1 (min^{-1})	$q_{e,\mathrm{cal}}$ (mg/g)	R^2	k_2 (g/mg min)	$q_{e,\mathrm{cal}}$ (mg/g)	R^2	k_p (mg/g min$^{0.5}$)	C (mg/g)	R^2
283	187.57	0.059	22.97	0.952	0.021	188.32	0.999	1.56	142.41	0.934
298	191.39	0.052	23.08	0.989	0.025	192.31	0.999	2.86	142.85	0.989
318	204.32	0.042	24.56	0.885	0.029	204.92	0.999	2.14	143.22	0.941

adsorption. The model can be described as the following equation [31]:

$$q_t = k_p t^{0.5} + c \tag{5}$$

where k_p (mg/(g min$^{0.5}$)) is the intraparticle diffusion rate constant, and c (mg/g) is the intercept of this equation.

The experimental data are fitted according to these kinetics models, the parameters are listed in Table 1. As the correlation coefficient (R^2) of pseudo-second-order model is much closer to 1.0 than other employed kinetic models, and the theoretical q_e values are also closer to the experimental ones, which indicates that the pseudo-second-order kinetic model is the most appropriate to interpret the adsorption process.

To further analyze the kinetic behavior, the activation energy of the adsorption was calculated based on Arrhenius equation, which is expressed as the following equation [32,33]:

$$\ln k_2 = -\frac{E_a}{RT} + \ln(A) \tag{6}$$

where k_2 is the rate constant of pseudo-second-order adsorption (g/(mg min)), as the adsorption kinetics is well described by this model; E_a is the activation energy of adsorption (kJ/mol); A is the Arrhenius factor; R is the universal gas constant (8.314 J/(mol K)); T is the temperature (K).

A plot of ln k_2 vs. $1/T$ yields a straight line, with slope $-E_a/R$. The value of E_a can be used to differentiate physical and chemical adsorptions. Physical adsorption can achieve equilibrium quickly, and the energy requirement is usually small, ranging from 5 to 40 kJ/mol [32,33]. Whereas chemical adsorption involves stronger interactions and requires higher activation energy, ranging from 40 to 800 kJ/mol [32,33]. The value of E_a based on calculation is 6.02 kJ/mol, indicating that the adsorption of MB onto MHA is a physical adsorption process and is consistent with the experimental results.

3.2.3. Adsorption isotherms

Adsorption isotherms of MB dye onto MHA at different temperatures are shown in Fig. 9. It is found that the amount of adsorbed MB increase with the increase of the reaction temperature, which indicates the adsorption is more favorable at higher temperature. To assess MB adsorption behavior on the MHA, the data were analyzed based on Langmuir, Freundlich, Sips, and Toth isothermal models.

Langmuir model is a commonly used model based on the assumption of a monolayer adsorption on a homogeneous surface [34]. The equation is expressed in Eq. (7):

$$\frac{C_e}{q_e} = \frac{1}{q_m b} + \frac{C_e}{q_m} \tag{7}$$

where q_e (mg/g) is the amount of MB adsorbed at equilibrium, C_e (mg/L) is the MB concentration at

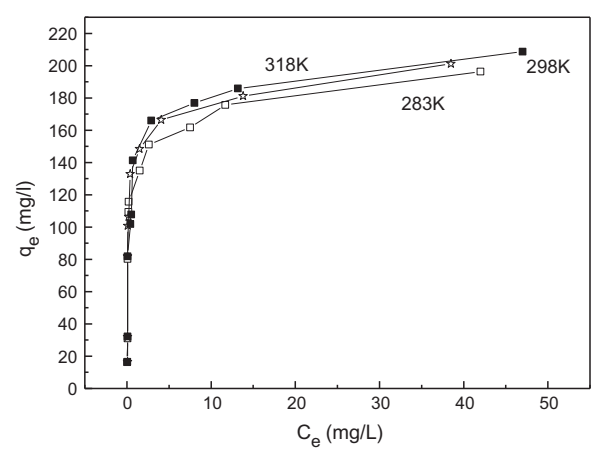

Fig. 9. Adsorption isotherms of MB onto MHA at various temperatures.

equilibrium, q_m (mg/g) is the maximum adsorption capacity when the adsorbent is fully covered, and b (L/mg) is the Langmuir adsorption constant which relates to the adsorption energy.

The linearized Freundlich isotherm model, which is valid for multilayer adsorption on a heterogeneous adsorbent surface with sites that have different energies of adsorption, is expressed in Eq. (8) [35]. Freundlich model is based on the assumption that adsorption energy decays exponentially with coverage rise [35]. Usually it is applied in the description of heterogeneous systems and is characterized by a heterogeneity factor, n [1].

$$\ln(q_e) = \ln(K_f) + \frac{1}{n}\ln(C_e) \tag{8}$$

where K_f is the Freundlich isotherm constant and n (dimensionless) is the heterogeneity factor. C_e is the equilibrium concentration (mg/L); q_e is the amount of MB adsorbed at equilibrium (mg/g).

Sips model is a modification of the Freundlich isotherms with consideration on the saturation of adsorption at high concentrations. It can be reduced to the Freundlich model at low concentration, but exhibits uptake limit for high concentrations [36]. The following equation gives the Sips model for adsorption in solutions:

$$q_e = \frac{b_s q_s C_e^{\frac{1}{s}}}{1 + q_s C_e^{\frac{1}{s}}} \tag{9}$$

where b_s (L/mg) is the Sips isotherm constant and s is Sips isotherm factor. C_e is the equilibrium concentration (mg/L); q_s (mg/g) is the Sips maximum adsorption capacity; q_e is the amount of MB adsorbed at equilibrium (mg/g).

Toth Model is a model assuming a Gaussian-like adsorption energy distribution [37]. Its expression is as Eq. (10):

$$q_e = \frac{K_t C_e}{(a_t + C_e)^{1/t}} \tag{10}$$

where a_t (mg/L), K_t and t are the Toth isotherm constants. C_e is the equilibrium concentration (mg/L); q_e is the amount of MB adsorbed at equilibrium (mg/g).

The simulation results based on the four models were listed in Table 2. According to Table 2, the correlation coefficients (R^2) of the linear form for Langmuir model are higher than those of other models at all the temperatures. Thus the isothermal adsorption behavior of MB onto MHA follows Langmuir equation, indicating a monolayer adsorption of MB occurring on a homogeneous surface.

Table 2
Isothermal parameters for the adsorption of MB onto MHA based on Langmuir, Freundlich, Sips, and Toth models

Model	Parameter	Temperature (K)		
		283	298	318
Langmuir	q_m (mg/g)	200	200	200
	b (L/mg)	1.67	2.50	1.67
	R^2	0.99	0.99	0.99
Freundlich	K_f	7.40	7.57	7.13
	n	3.77	3.88	4.27
	R^2	0.64	0.54	0.68
Sips	b_s (L/mg)	13.2	2.28	7.40
	q_s (mg/g)	168	201	181
	s	0.79	1.26	0.90
	R^2	0.87	0.93	0.84
Toth	K_t	150	161	166
	$a_t \times 10^2$ (mg/L)	8.9	17.2	12.6
	s	1.07	1.07	1.05
	R^2	0.90	0.94	0.85

To further investigate the isothermal behavior, a dimensionless constant of R_L, which reveals important characteristics of Langmuir model is calculated based on Eq. (11) [1,38]:

$$R_L = \frac{1}{(1 + bC_0)} \tag{11}$$

where C_0 (mg/L) is the initial MB concentration in solution. The value R_L indicates the tendency of adsorption process to be either unfavorable ($R_L > 1$), linear ($R_L = 1$), favorable ($0 < R_L < 1$), or irreversible ($R_L = 0$) [38]. Smaller R_L value indicates greater affinity between the adsorbent and the adsorbate [1]. The calculated R_L values in three temperatures are 0.029, 0.019, and 0.027 at the initial concentration of about 20 mg/L. These values are all much smaller than 1.0, indicating favorable adsorption for the MB at all the experimental conditions.

To further study the adsorption mechanism, thermodynamic parameters are calculated based on the following equations [32,33]:

$$\Delta G = -RT \ln b \tag{12}$$

Table 3
Thermodynamic parameters for the adsorption of MB onto MHA

ΔH (kJ/mol)	ΔS (J/mol K)	ΔG (kJ/mol)		
−7.77	87	283 K	298 K	318K
		−31.39	−34.07	−35.27

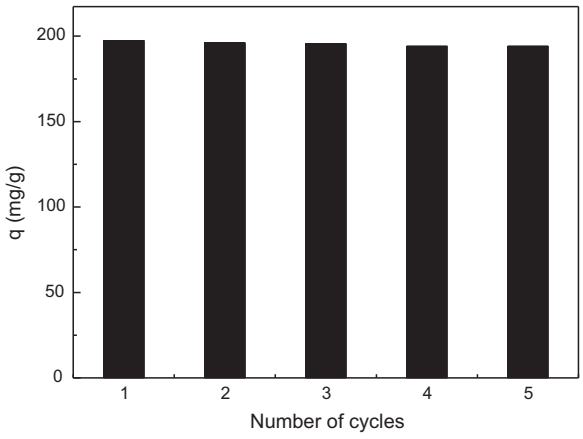

Fig. 10. Variation on adsorption capacity in regeneration cycles of MHA.

$$\Delta G = \Delta H - T\Delta S \tag{13}$$

where b is the thermodynamic distribution coefficient obtained from Langmuir model (L/mol); R is the universal gas constant (8.314 J/(mol K)); T is the temperature (K). ΔG (kJ/mol) is Gibbs free energy; ΔH (kJ/mol) is the enthalpy change; and ΔS (J/(mol K)) is the entropy change.

The thermodynamic parameters obtained based on Eqs. (12) and (13) are listed in Table 3. The values of ΔG at all the temperatures are negative, indicating that the adsorption of MB at these temperatures is spontaneous and thermodynamically favorable. The value of ΔH is negative, suggesting that the adsorption process is exothermic in nature. The positive value of ΔS indicates the affinity of MHA for MB and the disorder increase at the solid–liquid interface during the adsorption process.

3.3. Regeneration and reuse

The regeneration results are shown in Fig. 10. As shown in Fig. 10, the adsorption capacity of MB only experienced a very slight drop after five cycles. It suggested that the reusability of MHA is fine, which is satisfactory for practical applications.

4. Conclusion

In this work, magnetic Fe_3O_4/HA nanoparticles (MHA) was prepared using coprecipitation method. MHA shows fine magnetic response and high removal efficiency for MB in aqueous solution. TEM image indicates that MHA has a quasi-spherical structure feature with particle size of about 10 nm. The isoelectric point of MHA suspension is at the solution pH of 3.2. With a saturation magnetization of 62.88 μ/g, the MHA can be readily separated from its dispersion within a few minutes under a magnetic field. The adsorption equilibrium of MHA for adsorption of MB is achieved in 15 min and the adsorption kinetic process can be interpreted by pseudo-second-order model. The equilibrium adsorption data is in agreement with Langmuir isotherm model with a maximum adsorption amount of about 200 mg/g. The value of activation energy (E_a) indicates that the adsorption of MB onto MHA is a physical adsorption process. The value of Gibbs free energy (ΔG) is negative, indicating that the adsorption of MB onto MHA is spontaneous and thermodynamically favorable. Moreover, the reusability of MHA is fine as the adsorption capacity of MHA suffers little loss after five recycling cycles, which is satisfactory for practical applications.

Acknowledgements

This works was supported by the Project of Forestry Bureau of China (948 Program, Grant No. 2011-4-81), and the Priority Academic Program Development of Jiangsu Higher Education Institutions (PAPD).

References

[1] H. Yan, H. Li, H. Yang, A. Li, R. Cheng, Removal of various cationic dyes from aqueous solutions using a kind of fully biodegradable magnetic composite microsphere, Chem. Eng. J. 223 (2013) 402–411.
[2] V.K. Garg, R. Gupta, Basic dye (methylene blue) removal from simulated wastewater by adsorption using Indian rosewood sawdust: A timber industry waste, Dye Pig. 63 (2004) 243–250.
[3] B.H. Hameed, A.T.M. Din, A.L. Ahmad, Adsorption of methylene blue onto bamboo-based activated carbon: Kinetics and equilibrium studies, J. Hazard. Mater. 141 (2007) 819–825.
[4] R. Jiang, Y.Q. Fu, H.Y. Zhu, J. Yao, L. Xiao, Removal of methyl orange from aqueous solutions by magnetic maghemite/chitosan nanocomposite films: Adsorption kinetics and equilibrium, J. Appl. Polym. Sci. 125 (2012) 540–549.
[5] H.M.H. Gad, A.A. El-Sayed, Activated carbon from agricultural by-products for the removal of Rhodamine-B from aqueous solution, J. Hazard. Mater. 168 (2009) 1070–1081.

[6] F. Ferrero, Adsorption of methylene blue on magnesium silicate: Kinetics, equilibria and comparison with other adsorbents, J. Environ. Sci. 22 (2010) 467–473.
[7] L. Li, S. Liu, T. Zhu, Application of activated carbon derived from scrap tires for adsorption of Rhodamine B, J. Environ. Sci. 22 (2010) 1273–1280.
[8] M. Wawrzkiewicz, Anion exchange resins as effective sorbents for acidic dye removal from aqueous solutions and wastewaters, Solvent Extr. Ion Exch. 30 (2012) 507–523.
[9] G. Crini, Studies on adsorption of dyes on beta-cyclodextrin polymer, Bioresour. Technol. 90 (2003) 193–198.
[10] S.H. Chang, K.S. Wang, H.C. Li, M.Y. We, J.D. Chou, Enhancement of Rhodamine B removal by low-cost fly ash sorption with Fenton pre-oxidation, J. Hazard. Mater. 172 (2009) 1131–1136.
[11] K. Zhao, G. Zhao, P. Li, J. Gao, B. Lv, D. Li, A novel method for photodegradation of high-chroma dye wastewater via electrochemical pre-oxidation, Chemosphere 80 (2010) 410–415.
[12] J. Rajeev, M. Megha, S. Shalini, M. Alok, Removal of the hazardous dye Rhodamine B through photocatalytic and adsorption treatments, J. Environ. Manage. 85 (2007) 956–964.
[13] H. Yan, L. Yang, Z. Yang, H. Yang, A. Li, R. Cheng, Preparation of chitosan/poly(acrylic acid) magnetic composite microspheres and applications in the removal of copper(II) ions from aqueous solutions, J. Hazard. Mater. 229–230 (2012) 371–380.
[14] T.S. Anirudhan, C.D. Bringle, S. Rijith, Removal of uranium(VI) from aqueous solutions and nuclear industry effluents using humic acid-immobilized zirconium-pillared clay, Desalin. Water Treat. 12 (2009) 16–27.
[15] H.L. Pham, H.M. Do, D.L. Tran, V.H. Le, X.P. Nguyen, A.T. Nguyen, T.N. Nguyen, A.T. Vu, Magnetic nanoparticles: Study of magnetic heating and adsorption/desorption for biomedical and environmental applications, Int. J. Nanotechnol. 8 (2011) 399–413.
[16] J.F. Liu, Z.S. Zhao, G.B. Jiang, Coating Fe_3O_4 magnetic nanoparticles with humic acid for high efficient removal of heavy metals in water, Environ. Sci. Technol. 42 (2008) 6949–6954.
[17] W.H. Hendershot, M. Duquette, A simple barium chloride method for determining cation exchange capacity and exchangeable cations, Soil Sci. Soc. Am. J. 50 (1986) 605–608.
[18] L. Carlos, M. Cipollone, D.B. Soria, M.S. Moreno, P.R. Ogilby, F.S. García Einschlag, D.O. Martire, The effect of humic acid binding to magnetite nanoparticles on the photogeneration of reactive oxygen species, Sep. Purif. Technol. 91 (2012) 23–29.
[19] W. Yantasee, C.L. Warner, T. Sangvanich, R.S. Addleman, T.G. Carter, R.J. Wiacek, G.E. Fryxell, C. Timchalk, M.G. Warner, Removal of heavy metals from aqueous systems with thiol functionalized superparamagnetic nanoparticles, Environ. Sci. Technol. 41 (2007) 5114–5119.
[20] L. Peng, P.F. Qin, M. Lei, Q.R. Zeng, H.J. Song, J. Yang, J.H. Shao, B.H. Liao, J.D. Gu, Modifying Fe_3O_4 nanoparticles with humic acid for removal of Rhodamine B in water, J. Hazard. Mater. 209–210 (2012) 193–198.
[21] R.A. Alvarez-Puebla, J.J. Garrido, Effect of pH on the aggregation of a gray humic acid in colloidal and solid states, Chemosphere 59 (2005) 659–667.
[22] S.T. Yang, P.F. Zong, X.M. Ren, Q. Wang, X.K. Wang, Rapid and high-efficient preconcentration of Eu by core-shell structured Fe_3O_4@humic acid magnetic nanoparticles, ACS Appl. Mater. Interfaces 12 (2012) 6890–6899.
[23] E. Illes, E. Tombacz, The role of variable surface charge and surface complexation in the adsorption of humic acid on magnetite, Colloids Surf. A 230 (2003) 99–109.
[24] E. Illes, E. Tombacz, The effect of humic acid adsorption on pH-dependent surface charging and aggregation of magnetite nanoparticles, J. Colloid Interface Sci. 295 (2006) 115–123.
[25] H.Y. Niu, D. Zhang, S.X. Zhang, X.L. Zhang, Z.F. Meng, Y.Q. Cai, Humic acid coated Fe_3O_4 magnetic nanoparticles as highly efficient Fenton-like catalyst for complete mineralization of sulfathiazole, J. Hazard. Mater. 190 (2011) 559–565.
[26] L. Adamčíková, K. Pavlíková, P. Ševčík, The decay of methylene blue in alkaline solution, React. Kinet. Catal. Lett. 69 (2000) 91–94.
[27] I. Safarik, L. Rego, M. Borovska, E. Mosiniewicz-Szablewska, F. Weyda, M. Safarikova, New magnetically responsive yeast-based biosorbent for the efficient removal of water-soluble dyes, Enzym. Microb. Technol. 40 (2007) 1551–1556.
[28] R. Sutton, G. Sposito, Molecular structure in soil humic substances: The new view, Environ. Sci. Technol. 39 (2005) 9009–9015.
[29] S. Lagergren, About the theory of so-called sorption of soluble substances, Kung. Sven. Veten. Hand. 24 (1898) 1–39.
[30] Y.S. Ho, G. McKay, Sorption of dye from aqueous solution by peat, Chem. Eng. J. 70 (1998) 115–124.
[31] W.J. Weber, Kinetics of adsorption on carbon from solution, J. Sanit. Eng. Div. ASCE 89 (1963) 31–59.
[32] J.W. Lin, Y.H. Zhan, Z.L. Zhu, Adsorption characteristics of copper(II) ions from aqueous solution onto humic acid-immobilized surfactant-modified zeolite, Colloids Surf. A 384 (2011) 9–16.
[33] H.K. Boparai, M. Joseph, D.M. O'Carroll, Kinetics and thermodynamics of cadmium ion removal by adsorption onto nano zerovalent iron particles, J. Hazard. Mater. 186 (2011) 458–465.
[34] I. Langmuir, The adsorption of gases on plane surfaces of glass, mica and platinum, J. Am. Chem. Soc. 40 (1918) 1361–1402.
[35] H.M.F. Freundlich, Ueber die adsorption in loesungen, Z. Phys. Chem. 57 (1906) 385–470.
[36] R. Sips, On the structure of a catalyst surface, J. Chem. Phys. 16 (1948) 490–495.
[37] J. Toth, Adsorption Theory Modelling and Analysis, 1st ed., Dekker, New York, NY, 2002.
[38] S.T. Ong, E.H. Tay, S.T. Ha, W.N. Lee, P.S. Keng, Equilibrium and continuous flow studies on the sorption of Congo red using ethylenediamine modified rice hulls, Int. J. Phys. Sci. 4 (2009) 683–690.